COMPUTER METHODS AND PROGRAMS IN BIOMEDICINE 136 (2016) 89–96

journal homepage: www.intl.elsevierhealth.com/journals/cmpb

Intraoral radiographs texture analysis for dental implant planning

Mayara B.V. Mundim [a], *Danilo R. Dias* [a], *Ronaldo M. Costa* [b], *Cláudio R. Leles* [a], *Paulo M. Azevedo-Marques* [c], *Rejane F. Ribeiro-Rotta* [a,*]

[a] *School of Dentistry, Universidade Federal de Goias, Avenida Universitária esquina com 1a Avenida s/n, Setor Universitário, 74605-220 Goiânia, Goiás, Brazil*

[b] *Institute of Informatics, Universidade Federal de Goias, Alameda Palmeiras, Quadra D, Câmpus Samambaia, 74690-900 Goiânia, Goiás, Brazil*

[c] *Department of Internal Medicine, Ribeirão Preto Medical School, Universidade de São Paulo, Avenida Bandeirantes, n° 3900, Bairro Monte Alegre, 14048-900, Ribeirao Preto, São Paulo, Brazil*

ARTICLE INFO

Article history:
Received 28 February 2016
Received in revised form
23 July 2016
Accepted 18 August 2016

Keywords:
Dental implants
Implant stability
Computer-assisted diagnosis
Texture analysis
Image processing
Computer-assisted

ABSTRACT

Background and Objectives: Computer vision extracts features or attributes from images improving diagnosis accuracy and aiding in clinical decisions. This study aims to investigate the feasibility of using texture analysis of periapical radiograph images as a tool for dental implant treatment planning.

Methods: Periapical radiograph images of 127 jawbone sites were obtained before and after implant placement. From the superimposition of the pre- and post-implant images, four regions of interest (ROI) were delineated on the pre-implant images for each implant site: mesial, distal and apical peri-implant areas and a central area. Each ROI was analysed using Matlab® software and seven image attributes were extracted: mean grey level (MGL), standard deviation of grey levels (SDGL), coefficient of variation (CV), entropy (*En*), contrast, correlation (*Cor*) and angular second moment (ASM). Images were grouped by bone types—Lekholm and Zarb classification (1,2,3,4). Peak insertion torque (PIT) and resonance frequency analysis (RFA) were recorded during implant placement. Differences among groups were tested for each image attribute. Agreement between measurements of the peri-implant ROIs and overall ROI (peri-implant + central area) was tested, as well as the association between primary stability measures (PIT and RFA) and texture attributes.

Results: Differences among bone type groups were found for MGL ($p = 0.035$), SDGL ($p = 0.024$), CV ($p < 0.001$) and *En* ($p < 0.001$). The apical ROI showed a significant difference from the other regions for all attributes, except *Cor*. Concordance correlation coefficients were all almost perfect ($\rho > 0.93$), except for ASM ($\rho = 0.62$). Texture attributes were significantly associated with the implant stability measures.

Conclusion: Texture analysis of periapical radiographs may be a reliable non-invasive quantitative method for the assessment of jawbone and prediction of implant stability, with potential clinical applications.

* *Corresponding author*. School of Dentistry, Universidade Federal de Goias, Rua C-235 n.1323 apt.1501, Nova Suiça, Goiania 74280-130 Brazil. Fax: +55 62 32096067.

E-mail address: rejanefrr@gmail.com (R.F. Ribeiro-Rotta).

http://dx.doi.org/10.1016/j.cmpb.2016.08.012
0169-2607/

1. Background

Computer technology is a promising way to aid the health sciences [1–3], especially in the imaging diagnosis field and medical imaging interpretation process, which have received the greatest contribution from this tool [4]. Computer-aided diagnosis (CAD) can be defined as a diagnosis made by a professional who uses the automated result of quantitative analysis of images as a "second opinion" to improve diagnostic accuracy and aid in clinical decisions [4]. Among different areas of knowledge in CAD, the computer vision is the most commonly used in different specialties of health. It automatically extracts features or attributes from the images, visible or not to the human eye: density, contrast, magnification, sharpness, uniformity, density, roughness, intensity, etc [5–7].

Within the computer vision, the texture analysis is able to describe the spatial variations in intensity of grey levels. Thus, the texture method analyses local variations in pixel values that are regularly or randomly repeated along the image. The various techniques for texture analysis are distributed in four main groups: structural analysis, statistics, fractal and anisotropy [6]. Haralick and co-workers [6] characterised texture as a two-dimensional concept. One dimension contains primitive properties of grey levels (pixels) and the other corresponds to spatial relationships among them. These authors suggested one of the most efficient methods for texture analysis, the Haralick's method, which is in the statistical group. Based on this method, fourteen texture attributes can be analysed.

Texture analysis is widely used for bone tissue evaluation in patients with osteoporosis [8–10], and the fractal analysis method has been applied to evaluate jawbone sites in dentistry. The fractal dimension analysis has been pointed as a potential method to predict bone quality at dental implant sites [11] and has been tested to analyze changes on peri-implant alveolar bone after prosthodontic loading [12–15]. However, the statistical texture method is rarely used in dentistry to assess jawbone sites.

Jawbone characteristics may influence the success of implant treatment. Pre- and trans-operative methods have been used to measure bone characteristics for dental implant planning [16–18], including the subjective classification suggested by Lekholm and Zarb. These different methods provide morphometric aspects of bone, such as cortical thickness and trabecular density, which are related to mechanical anchorage of the implant during its placement. This implant stability at placement, defined as primary implant stability, has frequently been associated with successful implant treatment outcome [19]. Measurements of some bone morphological characteristics in a quantitative/objective way could contribute to predict primary implant stability and osseointegration success, particularly prior to invasive procedures. The aim of this study was to investigate the ability of statistical texture analysis performed in periapical radiographs of jawbone sites to identify the different bone types and predict primary implant stability.

2. Methods

2.1. Sample

Periapical radiographic images were obtained from forty-eight volunteers with an indication of dental implant treatment, selected according to clinical criteria, laboratory tests and radiographic images. One hundred and twenty-seven pre- and post-implant periapical images composed the sample of this study. Post implant radiographs were taken six months after implant placement.

Periapical radiographs were performed using Heliodent Dentotime (Siemens, Benshein, Germany) with the following parameters: 70 kVp, 10 mA, aluminium filter of 2.0 mm, rectangular collimator 3 x 4 cm, focus-film distance of 21 cm, exposure time ranging between 0.25–0.4 s. E-speed dental films (Kodak Ektaspeed, Eastman Kodak Co., Rochester, NY) were used and processed automatically (Peri-Pro, Air Maintenance Techniques, USA) with a cycle of 6 minutes at 27°C.

The conventional radiographs were digitalised using a Sony Cyber-Shot DSC-W210 digital camera with 12.1 megapixel resolution and 2X optical zoom. Images were obtained with standardised criteria of lens–film distance and lightness, and saved in JPEG format, with 256 gray levels.

2.2. Subjective bone classification and implant stability measurements

The subjective bone classification, according to Lekholm and Zarb [19] criteria (bone types 1, 2, 3 and 4), was performed by the three oral surgeons who placed the implants. Each surgeon evaluated only the sites to be operated by himself, since Lekholm and Zarb classification [19] required radiographic interpretation associated with tactile perception of the surgeon during the drilling of the bone site, which does not allow simultaneous classification by more than one surgeon. The surgeons received a calibration card with schematic design and description of the bone type classification according to Lekholm and Zarb (Fig. 1), which serves as a reference (calibration) during each reading. They registered their subjective rate of each implant site in the patient's records. So, bone classification was carried out in two steps: at first, a radiographic imaging interpretation was performed based on periapical and panoramic images, under favourable light conditions, using a schematic bone type drawing [19] as a reference. During surgery, the final bone classification was established based on previous radiographic interpretation associated with the surgeon's tactile perception of bone resistance at first drilling for implant installation (Fig. 1).

Implants were installed using the two stage protocol [20,21]. Trans-operative implant stability measurements were collected: peak-insertion torque (PIT) and implant stability quotient (ISQ). PIT was recorded by the surgical micromotor display (BLM 600 Plus, Driller, Sao Paulo, SP, Brazil) at 1300 rpm for the initial drill hole. These values ranged from 15 to 55 Ncm. When final anchorage required a torque higher than 55 Ncm, this was achieved by a manual wrench (Neodent, Curitiba, Brazil).

Resonance frequency analysis (RFA) was performed immediately after implant insertion using a wireless device, the

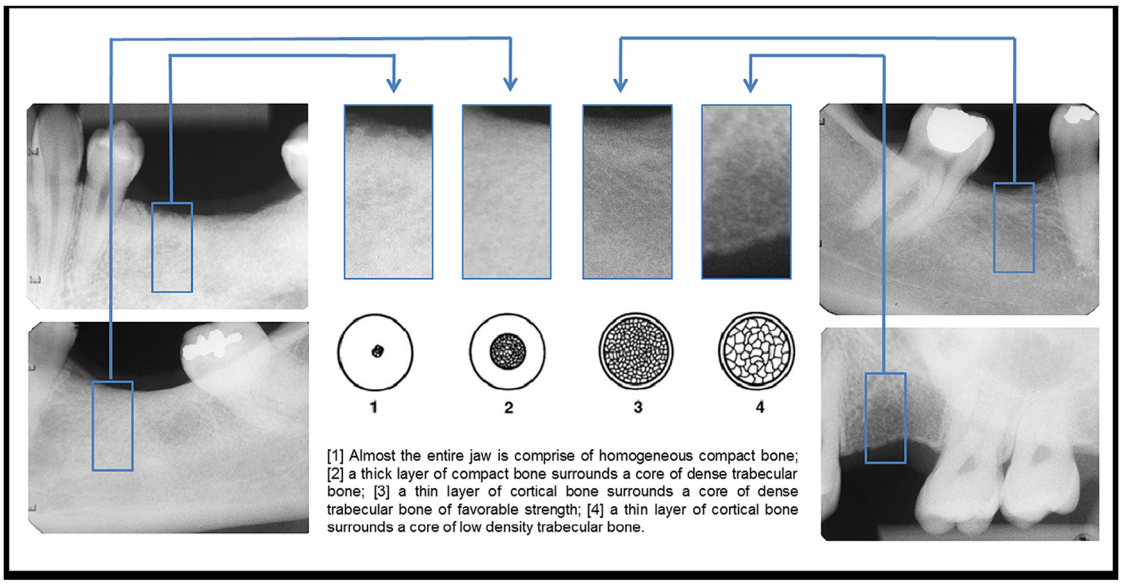

Fig. 1 – Jawbone site radiographic images according to Lekholm and Zarb's bone classification. Original description according to Lekholm and Zarb with kind permission from Quintessence Publishing Co. Inc.

Osstell™ Mentor (Osstell AB—Integration Diagnosis, Gothenburg, Sweden). The resonance frequency was measured by positioning the device's probe perpendicular to a transductor attached to the implant (Smartpeg, Integration Diagnostics AB, Gothenburg, Sweden). The device automatically converts the signal into a quotient—the ISQ. The higher the ISQ (1 to 100), the more stable the implant is.

2.3. *Texture analysis*

The periapical digitalised radiographic images were transferred to a desktop computer. The regions of interest (ROI) were defined by superimposing pre- and post-implant installation images of the same site, using the Adobe Photoshop CS6 software (Adobe, California, USA). Four ROIs with pre-established sizes (see Fig. 2) were selected in pre-implant images for each implant site position: "c" region, which corresponds to the central bone specimen removed during the implant placement; "m", the mesial peripheral region of the implant; "d", the distal peripheral region of the implant; and "a", the apical peripheral region of the implant. Each ROI was cut and saved as a 256 gray level PNG image (8 bits) (Portable Network Graphics) and submitted to Matlab R2012b software for Linux (MathWorks Inc., Natick, MA, USA) for image texture attribute extraction. ROI selection was done by the same examiner (first author), and the calibration process was performed in other images that were not included in the sample.

Three statistical parameters were obtained: mean and standard deviation of grey levels and coefficient of variation. Four image texture attributes derived from a co-occurrence matrix calculated with one pixel distance and 0°, 45°, 90° and 135° directions, based on Haralick's method [6], were obtained: contrast, correlation, entropy and angular second moment (Table 1). These texture attributes have been used the most in recent health approaches. A mean vector of each of the statistical parameters and image texture attributes was calculated considering each selected ROI ("c" + "m" + "d" + "a") for each pre-implant image, resulting in statistical parameters and image texture attributes for an overall ROI. Individual ROIs and overall ROIs were grouped according to bone types 1, 2, 3 and 4 and a new mean vector was calculated for each attribute in order to characterise those bone types.

2.4. *Data analysis*

Mean and standard deviation were calculated for all texture attributes for the overall ROI ("c" + "m" + "d" + "a") and for the subgroups of bone type classifications (1, 2, 3, 4). One-way ANOVA and the Kruskal–Wallis test were used for group comparison to test differences between bone type groups. Statistical significance was set at $p < 0.05$.

The concordance correlation coefficients, ρ_c, between the peri-implant and overall ROI, were calculated for each texture attribute to measure the degree to which pairs of observations fall on the 45° line through the origin. It contains a measurement of precision ρ and accuracy C_b, where ρ is the Pearson correlation coefficient, which measures how far each observation deviates from the best-fit line (measure of precision), and C_b is a bias correction factor that measures how far the best-fit line deviates from the 45° line through the origin (measure of accuracy).

Multiple linear regression was performed for the association between primary stability measures (PIT and ISQ) and texture analysis attributes.

Data analysis was performed using the MedCalc 12.3.0 software (MedCalc Software, Acacialaan 22, B-8400 Ostend, Belgium).

3. Results

The demographic profile of the 48 patients (127 bone implant sites) consisted of 30 females (62.5%), with a mean age of 43.02

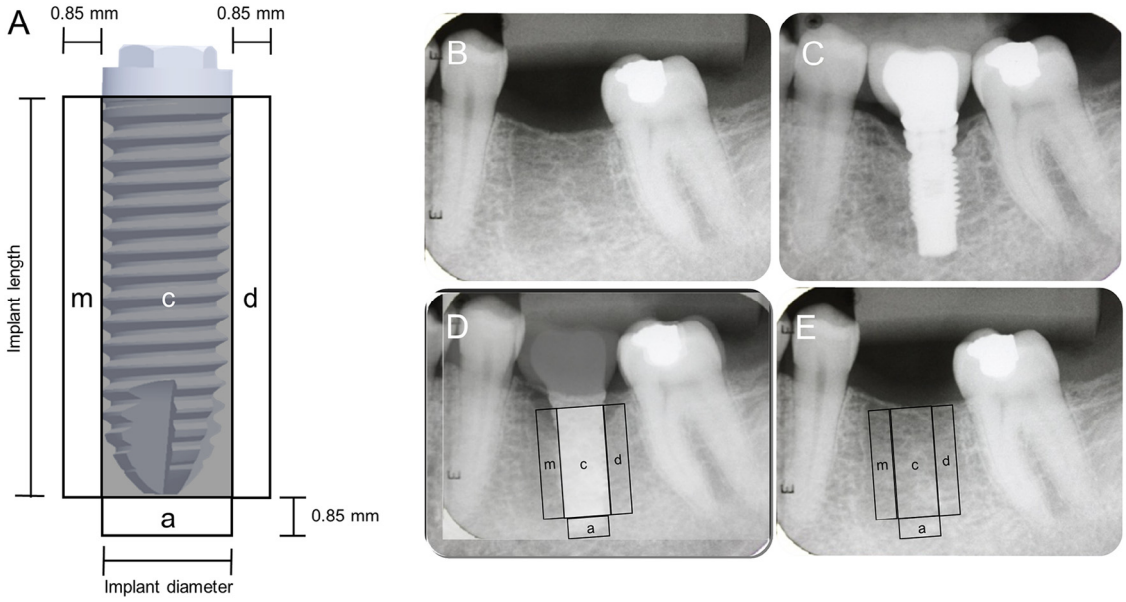

Fig. 2 – ROI dimensions: A) Central region ("c") was established according to the different dimensions of the implants installed. To the peri-implant regions "m" and "d", a fixed width of 0.85 mm and a variable height, depending on the implant length, were considered. To the images of peri-implant apical region "a", a fixed height of 0.85 mm and a variable width, depending on the implant diameter, were considered. ROI selection process in the digitalised periapical images: B) pre-implant periapical radiograph; C) post-implant periapical radiograph; D) pre and post-implant periapical radiographs superimposed with ROI delimitation; E) pre-implant periapical radiograph with ROI delimitation to proceed to texture analysis.

years (SD = 10.27). The implant sites were distributed in maxilla (39.4%) and mandible (60.6%). The distribution of bone type classifications is described in Table 2. Most of the implant sites were classified as bone types 2 and 3 (70.1%).

The 508 ROIs marked in 127 periapical radiographs were evaluated for texture analysis and five of the seven extracted image parameters/attributes presented normal and two non-normal distributions (Kolmogorov–Smirnov test). The one-way ANOVA (Table 2) revealed a statistically significant difference between the parameters/attributes mean grey level, standard deviation and entropy ($p < 0.05$) when comparing the four bone types. The Kruskal–Wallis test was performed with coefficient of variation and correlation. Coefficient of variation presented a statistically significant difference ($p < 0.001$) between the four bone types (Table 3).

It was observed that bone type 1 presented a wider number of grey levels with less variation between them and greater textural homogeneity. Bone type 4 showed a smaller number of

Table 1 – Definitions and formulae of texture analysis attributes.

Attribute	Definition	Formulae
Mean grey level	Measure of the arithmetic mean of pixels values in the ROI	$me = \frac{\sum pv}{N(pv)}$
Standard deviation	Measure of variation or dispersion that exists in the pixels values mean	$sd = \frac{\sqrt{\sum (pv1 - pv)2}}{N(pv) - 1}$
Coefficient of variation	Measure of the ratio between standard deviation and the mean grey level	$cv = \frac{sd}{me}$
Contrast	Measure of the amount of local variations present in an image	$con = \sum_{i=1}^{n}\sum_{j=1}^{n} \frac{(i-j)^2 . p(i,j,d,\theta)}{i.j}$
Correlation	Measure of grey-tone linear-dependencies in the image	$cor = \frac{\sum_{i=1}^{n}\sum_{j=1}^{n} \frac{(i-j)^2 . p(i,j,d,\theta)}{i.j} - \mu i.\mu j}{\sigma i.\sigma j}$
Entropy	Measure of randomness of grey-tone in the image	$ent = \sum_{i=1}^{n}\sum_{j=1}^{n} \frac{p(i,j,d,\theta)}{i.j} . \log\left(\frac{i.j}{p(i,j,d,\theta)}\right)$
Angular second moment	Measure of homogeneity of the image	$asm = \sum_{i=1}^{n}\sum_{j=1}^{n} \left(\frac{p(i,j,d,\theta}{i.j}\right)^2$

Table 2 – Mean (and standard deviation) of parametric statistical parameters and texture attributes of overall ROI, according to bone type classification (n = 127).

Bone type	n (%)	Mean grey level	Standard deviation	Entropy	Contrast ($\times 10^3$)	ASM ($\times 10^{-5}$)
1	11 (8.7)	178.8 (37.0)	15.0 (6.1)	5.40 (0.4)	25.6 (11.8)	13.0 (2.9)
2	42 (33.1)	140.2 (40.2)	13,8 (4.9)	5.40 (0.5)	29.2 (13.0)	13.7 (3.0)
3	47 (37.0)	137.4 (46.7)	16,1 (6.1)	5.64 (0.5)	31.9 (13.5)	13.6 (3.1)
4	27 (21.3)	134.0 (49.8)	18.0 (5.0)	5.92 (0.4)	25.4 (10.0)	15.2 (4.2)
P-value	–	0.035	0.024	<0.001	0.143	0.125

One-way ANOVA test.

grey levels, with a wider variation among them and greater heterogeneity. Bone types 2 and 3 revealed intermediate characteristics for the three attributes. Nevertheless, a wider range of gray tones was observed in type 3 when compared to type 2 (Tables 2 and 3).

In the evaluation of each ROI individually (Table 4), the apical ROI ("a") showed a statistically significant difference for all of the attributes except for correlation.

Concordance correlation coefficient between overall and peri-implant ROI ranged from substantial to almost perfect concordance ($\rho = 0.93–0.99$), except for angular second moment, which presented poor concordance ($\rho = 0.62$).

Regression analysis showed that five evaluated parameters (mean grey level, standard deviation, coefficient of variation, correlation and entropy) were significantly associated with implant stability measures (Table 5).

4. Discussion

The main contribution of this study to dental implant planning was to identify that periapical image texture analysis can differentiate the four bone types, according to a worldwide known subjective classification [19,22]. Furthermore, the image attributes are associated with implant stability.

The consistency of the main findings of this study can be observed if a parallel analysis is done, considering Lekholm and Zarb's description of the four bone types [19], and the results of the four image attributes (mean grey level, standard deviation, entropy and coefficient of variation) that significantly differentiated these bone types (Tables 2, 4).

Bone type 1, which is mainly cortical [19] and has a more radiopaque x-ray image, should have a narrower grey scale (entropy) with a slight variation of its pixel values from the mean (standard deviation). This bone type presented a high mean grey level with little variation in pixels values, which determines the small values of the ratio between the attributes standard deviation and the mean grey levels (coefficient of variation = $cv = \frac{sd}{me}$). Furthermore, bone types 2, 3 and 4, which gradually increase the predominance of wider medullar spaces and radiographic radiolucency, also gradually increase their grey scale (entropy) and the variation of pixel values relative to the mean (standard deviation). Therefore, these bone types will show a gradually lower mean grey level and larger variation of their pixels values, thereby determining a higher coefficient of variation from bone types 2 to 4.

Table 3 – Mean (and standard deviation) of non-parametric statistical parameters and texture attributes of overall ROI, according to bone type classification (n = 127).

Bone type	n (%)	Coefficient of variation ($\times 10^{-2}$)	Correlation ($\times 10^{-5}$)
1	11 (8.7)	8.5 (2.8)	31.0 (57.0)
2	42 (33.1)	11.1 (5.7)	18.7 (52.6)
3	47 (37.0)	14.2 (8.6)	0.08 (111.6)
4	27 (21.3)	17.2 (11.0)	4.01 (74.8)
P-value	-	<0.001	0.652

Among the texture attributes extracted, entropy was the one that more significantly distinguished bone types ($P < 0.001$), which is in line with studies evaluating other anatomical regions, such as the femur of patients with osteoporosis [23].

Primary implant stability, which indicates stability at implant placement, has been highlighted as a key to implant success outcome and has been related to bone quality [24–26]. Such information may be used in the planning phase to predict the optimum healing period and point at which an implant may be suitable for loading [27].

Subjective bone classification is used to predict primary implant stability, while peak insertion torque and resonance frequency analysis are among the most commonly used methods to measure this stability. Peak insertion torque and resonance frequency analysis cannot be measured before the implant placement, and only the last one allows longitudinal implant stability measurements [27–29]. As well, subjective bone classification according to Lekholm and Zarb [19] depends on surgeon tactile perception of bone resistance at first drilling for implant placement. Thus, all of these mainly methods to predict implant success based on primary implant stability depend on some information taken at surgery moment. In this study, periapical image texture attributes added information on differentiating bone types, and still showed an association with peak insertion torque and resonance frequency analysis measurements. Therefore, as a non-invasive test that uses routine radiographs for implant planning, with accessibility and economic viability, it can be considered a promising and potential tool to be included in clinical routine.

Regarding the ROI selection for texture measurements, the fact that the results showed no difference between selecting specific peri-implant regions compared to the overall ROI might represent a positive factor for texture analysis as a tool for dental implant planning. This becomes even more important in consecutive multiple implants, when the examiner would probably have more of a chance of making an error in subjective

Table 4 – Descriptive statistics of mean, standard deviation and variation coefficient of gray levels and texture attributes of each region of interest according to bone type.

	n	Grey levels			Texture attributes			
		Mean M (±SD)	Standard Deviation M (±SD)	Variation coefficient M (±SD)	Contrast ($\times 10^{2}$) M (±SD)	Correlation ($\times 10^{-4}$) M (±SD)	Entropy M (±SD)	Angular second moment ($\times 10^{-4}$) M (±SD)
Bone type 1	11							
Apical region		191.29(±43.96)	6.43(±1.23)	0.04(±0.01)	66.4(±37.12)	–0.06(±12.29)	4.65(±0.28)	2.62(±0.53)
Central region		177.36(±36.48)	18.79(±8.96)	0.11(±0.04)	210.37(±96.69)	–5.12(±14.43)	5.81(±0.5)	0.16(±0.06)
Distal region		177.07(±33.41)	16.45(±9.29)	0.09(±0.05)	364.02(±174.42)	–2.16(±4.05)	5.48(±0.7)	1.21(±0.36)
Mesial region		169.49(±36.4)	18.21(±9.53)	0.11(±0.05)	382.53(±184.03)	–5.05(±6.7)	5.66(±0.55)	1.2(±0.32)
Bone type 2	42							
Apical region		152.07(±41.73)	6.23(±3)	0.04(±0.02)	46.03(±17.01)	1.19(±14.07)	4.46(±0.66)	3.06(±0.76)
Central region		133.99(±41.23)	17.7(±7.02)	0.15(±0.08)	260.72(±125.48)	–2.63(±10)	5.9(±0.55)	0.17(±0.1)
Distal region		138.5(±40.37)	14.99(±6.73)	0.12(±0.06)	421.18(±200.67)	–3.63(±7.67)	5.56(±0.61)	1.12(±0.31)
Mesial region		136.1(±41.05)	16.46(±7.23)	0.14(±0.10)	438.29(±201.33)	–2.41(±5.29)	5.7(±0.54)	1.11(±0.29)
Bone type 3	47							
Apical region		153.27(±47.97)	7.77(±2.88)	0.06(±0.08)	51.38(±38.97)	3.26(±24.32)	4.83(±0.57)	2.99(±0.65)
Central region		130.29(±48.22)	19.94(±8.96)	0.18(±0.1)	280.38(±140.34)	–1.18(±14.55)	6.04(±0.68)	0.17(±0.13)
Distal region		137.93(±47.93)	17.09(±8.96)	0.15(±0.11)	474.38(±210.85)	–3.99(±8.05)	5.71(±0.68)	1.14(±0.41)
Mesial region		128(±46.09)	19.5(±8.57)	0.18(±0.9)	469.53(±207.1)	1.88(±17.71)	5.97(±0.6)	1.13(±0.36)
Bone type 4	27							
Apical region		155.02(±54.43)	9.36(±3.43)	0.08(±0.07)	43.58(±18.54)	–0.27(±23.61)	5.11(±0.58)	3.31(±0.86)
Central region		125.07(±49.8)	21.21(±6.88)	0.21(±0.14)	210.12(±91.61)	1.6(±6.4)	6.26(±0.53)	0.19(±0.13)
Distal region		133.68(±48.27)	21.63(±6.98)	0.19(±0.1)	376.77(±152.05)	–6.96(±20.93)	6.20(±0.47)	1.27(±0.41)
Mesial region		122.08(±49.7)	19.76(±7.15)	0.21(±0.16)	386.27(±174.35)	4.02(±20.83)	6.1(±0.54)	1.32(±0.47)

Table 5 – Association between primary stability measures and texture analysis attributes (multiple linear regression parameters).

Texture attributes	Standardised regression coefficient (p-value)	
	Peak insertion torque	Resonance frequency
Entropy	–0.66 (0.001)	–0.92 (<0.001)
Standard deviation	0.47 (0.022)	0.59 (0.005)
Mean grey level	0.24 (0.006)	Ns
Correlation	–0.23 (<0.001)	–0.18 (0.036)
Variation coefficient	Ns	–0.24 (0.009)

Kruskal–Wallis test.

bone classification of each site individually. In this case, only the trans-operative tactile perception could provide information regarding implant selection, its prognosis and loading time.

We could not find a reasonable explanation for the divergent results found in the attributes extracted from apical ROI compared to others. A possible hypothesis could be that the apical region of the implant is located beyond the alveolar process and in a two-dimensional radiographic image; it could be overlapped by other structures and/or anatomical variations, generating significant pixels changes and consequent alterations in the texture attributes.

Some authors [30] have shown a difference in texture analysis values when comparing direct digital images and scanned images. The explanation for this difference was attributed to the cut-out of the number of steps used in the assessment of the texture parameters. Direct digital images are obtained without film processing or imaging digitalization. This reduces the loss of image information, enhancing the reproducibility of texture parameter measurements [30]. The present study used digitalized periapical radiographs, which may represent a limitation. On the other hand, it is important to point out that using periapical film the patient will receive a low radiation dose when compared with other radiograph modalities used for implant planning, as panoramic images or cone-beam computed tomography [31]. Further studies, using direct digital images [30] and comparison with morphometric referential methods [9], can provide a better understanding with regard to periapical image texture analysis as a tool for evaluating jawbone characteristics.

5. Conclusions

In summary, the results of this study can be divided into three prominent findings in terms of the use of texture analysis of periapical radiographs for implant treatment planning: a) most of the texture attributes allow differentiation between the four bone types (1, 2, 3 and 4); b) although the attributes in the apical ROI had shown divergent values from the other ROIs, the ROI selection for attribute extraction suffered no influence from segmented selection or overall area selection; and c) there was an association between five image attributes (entropy, standard deviation, mean grey level, correlation and variation coefficient) and the implant stability measures tested.

Texture analysis of periapical radiographs can be considered a potential method to assess jawbone tissue for dental implant planning.

Conflict of interest

The authors declare that there is no conflict of interest for this study.

Acknowledgment

This study was approved by the Ethical Committee at Federal University of Goias, Brazil (114/2007). Informed consent was obtained from all volunteers.

Supported by CNPq 483867/2011-0 (National Counsel of Technological and Scientific Development), ILAPEO/2007 (Instituto Latino Americano de Pesquisa e Ensino em Odontologia) and by FAPEG Ch02/2007 (Fundação de Amparo à Pesquisa do Estado de Goiás).

REFERENCES

[1] Q. Gao, J. Yu, F. Wang, T. Ge, L. Hu, Y. Liu, Automatic measurement of skin textures of the dorsal hand in evaluating skin aging, Skin Res. Technol. 19 (2) (2013) 145–151.

[2] G. Bahl, I. Cruite, T. Wolfson, A.C. Gamst, J.M. Collins, A.D. Chavez, et al., Noninvasive classification of hepatic fibrosis based on texture parameters from double contrast-enhanced magnetic resonance images, J. Magn. Reson. Imaging 36 (2012) 1154–1161.

[3] A. Padma, R. Sukanesh, Combined texture feature analysis of segmentation and classification of benign and malignant tumour CT slices, J. Med. Eng. Technol. 37 (1) (2012) 1–9.

[4] M.L. Giger, Computerized analysis of images in the detection and diagnosis of breast cancer, Semin. Ultrasound CT MR 25 (2004) 411–418.

[5] M.C. Barretto, D.A. Kulkarni, G.R. Udupi, A texture analysis method for detection of clustered microcalcifications on digital mammograms, Int. J. Bioinform. Res. Appl. 8 (2012) 366–381.

[6] R.M. Haralick, K. Shanmugam, I. Dinstein, Textural features for image classification, IEEE Trans. Inf. Technol. Biomed. 3 (1973) 610–621.

[7] E. Lespessailles, C. Chappard, N. Bonnet, C.L. Benhamou, Imaging techniques for evaluating bone microarchitecture, Joint Bone Spine 73 (2006) 254–261.

[8] L. Apostol, V. Boudousq, O. Basset, C. Odet, S. Yot, J. Tabary, et al., Relevance of 2D radiographic texture analysis for the assessment of 3D bone micro-architecture, Med. Phys. 33 (2006) 3546–3556.

[9] D. Chappard, P. Guggenbuhl, E. Legrand, M.F. Basle, M. Audran, Texture analysis of X-ray radiographs is correlated with bone histomorphometry, J. Bone Miner. Metab. 23 (2005) 24–29.

[10] T. Le Corroller, M. Pithioux, F. Chaari, B. Rosa, S. Parratte, B. Maurel, et al., Bone texture analysis is correlated with three-dimensional microarchitecture and mechanical properties of trabecular bone in osteoporotic femurs, J. Bone Miner. Metab. 31 (1) (2012) 82–88.

[11] B.T. Suer, Z. Yaman, B. Buyuksarac, Correlation of fractal dimension values with implant insertion torque and resonance frequency values at implant recipient sites, Int. J. Oral. Maxillofac. Implants 31 (2016) 55–62.
[12] O. Gonzalez-Martin, E.A. Lee, M. Veltri, CBCT fractal dimension changes at the apex of immediate implants placed using undersized drilling, Clin. Oral Implants Res. 23 (2012) 954–957.
[13] T.J. Mu, D.W. Lee, K.H. Park, I.S. Moon, Changes in the fractal dimension of peri-implant trabecular bone after loading: a retrospective study, J. Periodontal. Implant. Sci. 43 (2013) 209–214.
[14] E. Onem, B.G. Baksi, E. Sogur, Changes in the fractal dimension, feret diameter, and lacunarity of mandibular alveolar bone during initial healing of dental implants, Int. J. Oral Maxillofac. Implants 27 (2012) 1009–1013.
[15] M. Zeytinoglu, B. Ilhan, N. Dundar, H. Boyacioglu, Fractal analysis for the assessment of trabecular peri-implant alveolar bone using panoramic radiographs, Clin. Oral Investig. 19 (2015) 519–524.
[16] D. Chappard, Bone microarchitecture, Bull. Acad. Natl Med. 194 (2010) 1469–1480, discussion 1480-1461.
[17] D. Chappard, M.F. Basle, E. Legrand, M. Audran, Trabecular bone microarchitecture: a review, Morphologie 92 (2008) 162–170.
[18] D. Chappard, M.F. Basle, E. Legrand, M. Audran, New laboratory tools in the assessment of bone quality, Osteoporos. Int. 22 (2011) 2225–2240.
[19] U. Lekholm, G.A. Zarb, Patient selection and preparation, in Tissue integrated prostheses: osseointegration in clinical dentistry, Quintessence Publishing Co., Chicago, IL, 1985, pp. 199–209.
[20] P.I. Branemark, R. Adell, U. Breine, B.O. Hansson, J. Lindstrom, A. Ohlsson, Intra-osseous anchorage of dental prostheses. I. Experimental studies, Scand. J. Plast. Reconstr. Surg. 3 (1969) 81–100.
[21] G.C. Smith, Surgical principles of the Branemark osseointegration implant system, Aust. Prosthodont. Soc. Bull. 15 (1985) 37–40.
[22] R.F. Ribeiro-Rotta, A.C. Pereira, G.H. Oliveira, M.C. Freire, C.R. Leles, C. Lindh, An exploratory survey of diagnostic methods for bone quality assessment used by Brazilian dental implant specialists, J. Oral Rehabil. 37 (2010) 698–703.
[23] P. Ranjanomennahary, S.S. Ghalila, D. Malouche, A. Marchadier, M. Rachidi, C. Benhamou, et al., Comparison of radiograph-based texture analysis and bone mineral density with three-dimensional microarchitecture of trabecular bone, Med. Phys. 38 (2011) 420–428.
[24] B. Friberg, T. Jemt, U. Lekholm, Early failures in 4,641 consecutively placed Branemark dental implants: a study from stage 1 surgery to the connection of completed prostheses, Int. J. Oral Maxillofac. Implants 6 (1991) 142–146.
[25] I.H. Orenstein, D.P. Tarnow, H.F. Morris, S. Ochi, Three-year post-placement survival of implants mobile at placement, Ann. Periodontol. 5 (2000) 32–41.
[26] L. Sennerby, J. Roos, Surgical determinants of clinical success of osseointegrated oral implants: a review of the literature, Int. J. Prosthodont. 11 (1998) 408–420.
[27] N. Meredith, Assessment of implant stability as a prognostic determinant, Int. J. Prosthodont. 11 (1998) 491–501.
[28] R.F. Ribeiro-Rotta, C. Lindh, A.C. Pereira, M. Rohlin, Ambiguity in bone tissue characteristics as presented in studies on dental implant planning and placement: a systematic review, Clin. Oral Implants Res. 22 (2011) 789–801.
[29] R.F. Ribeiro-Rotta, C. Lindh, M. Rohlin, Efficacy of clinical methods to assess jawbone tissue prior to and during endosseous dental implant placement: a systematic literature review, Int. J. Oral Maxillofac. Implants 22 (2007) 289–300.
[30] E. Lespessailles, C. Gadois, G. Lemineur, J.P. Do-Huu, L. Benhamou, Bone texture analysis on direct digital radiographic images: precision study and relationship with bone mineral density at the os calcis, Calcif. Tissue Int. 80 (2007) 97–102.
[31] S. Han, B. Lee, G. Shin, J. Choi, J. Kim, C. Park, et al., Dose area product measurement for diagnostic reference levels and analysis of patient dose in dental radiography, Radiat. Prot. Dosimetry 150 (2012) 523–531.